

A General Formulation of the Kinematic Dipole as a Functional of Selection and Source Properties: Beyond the Ellis–Baldwin Approximation

TSUTOMU T. TAKEUCHI  ^{1, 2}

¹ *Division of Particle and Astrophysical Science, Nagoya University, Japan*

² *The Research Center for Statistical Machine Learning, the Institute of Statistical Mathematics, Japan*

ABSTRACT

The dipole anisotropy in galaxy and QSO number counts induced by the motion of the observer (the kinematic dipole) provides an important test of cosmological isotropy and a comparison with the Cosmic Microwave Background (CMB) dipole. Traditionally, the Ellis & Baldwin expression, $\mathcal{A} = 2 + x(1 + \alpha)$, has been widely adopted, assuming power-law number counts and a single power-law spectral energy distribution (SED). Realistic surveys, however, involve a range of non-ideal effects, including diverse SEDs, finite instrumental bandpasses, non-power-law number counts, multi-band photometry and photo- z selections, and direction-dependent or stochastic detection limits. In this paper, we incorporate these effects explicitly at the theoretical level and present a unified formulation of the kinematic dipole for a general parent population and a general multi-dimensional selection function. We show that the dipole amplitude is not described by a single index, but is instead given by a functional, $\mathcal{A}[\mathcal{W}, f]$, defined as the Doppler response of the selection function acting on the underlying population. We demonstrate that the classical Ellis–Baldwin result is recovered as a special limiting case of this formalism, and clarify the relation between the theoretical coefficient \mathcal{A} and the dipole vector estimated from finite catalogs, separating theoretical response from statistical uncertainty. This framework provides a basis for reinterpreting reported discrepancies in kinematic dipole measurements across surveys and is directly applicable to future wide-area, multi-band observations.

Keywords: Cosmic isotropy (320) — Cosmic microwave background radiation (322) — Cosmology (343) — Doppler shift (401) — Galaxies (573) — Large-scale structure of the universe (902)

1. INTRODUCTION

Extragalactic source counts, such as those of galaxies and QSOs (quasi-stellar objects), provide a fundamental probe of large-scale isotropy on the sky. If the sources are statistically isotropic in the cosmic rest frame, the motion of the observer with velocity

$$\vec{\beta} \equiv \vec{v}/c \quad (1)$$

induces a characteristic dipolar modulation in the observed number counts. This so-called *kinematic dipole* arises from two simultaneous relativistic effects: (i) the transformation of solid angle due to aberration, and (ii) Doppler boosting of the observed fluxes, together with the resulting deformation of the selection criteria. The first systematic formulation of this effect was given by [G. F. R. Ellis & J. E. Baldwin \(1984\)](#), who showed that, under the assumptions that the cumulative number counts follow a power law, $N(> S) \propto S^{-x}$, and that the source spectrum can be approximated by a single power law, $S_\nu \propto \nu^{-\alpha}$, the dipole coefficient \mathcal{A} is given by

$$\mathcal{A} = 2 + x(1 + \alpha). \quad (2)$$

Subsequent studies, primarily focusing on radio surveys, have examined in detail how practical aspects of data analysis such as sky masks, survey completeness, flux calibration, and the bias and variance of dipole estimators affect

the inferred kinematic dipole (e.g. F. Crawford 2009; M. Rubart & D. J. Schwarz 2013; P. Tiwari et al. 2015). More recently, systematic comparisons between different estimators (number-count dipoles versus sky-brightness dipoles, choices of weighting schemes, and flux-threshold dependence) have been carried out, together with assessments of consistency or tension with the CMB dipole (e.g. T. M. Siewert et al. 2021). Beyond radio wavelengths, kinematic dipole analyses based on optical and infrared QSO catalogs have also been reported, including studies using wide-area infrared QSO samples (e.g., A. K. Singal 2021; N. J. Secrest et al. 2021) and emission-line galaxy catalogs (K. Ahn 2025).

At the same time, the origin of the CMB dipole itself has been revisited, in particular whether it can be fully explained as a purely kinematic effect or may contain an intrinsic component. In this context, extragalactic source-count dipoles provide an important independent test of the standard interpretation (e.g. P. d. S. Ferreira & M. Quartin 2021). A systematic observational study of dipoles in projected large-scale structure was presented by C. Gibelyou & D. Huterer (2012), who analyzed number-count dipoles across multiple all-sky surveys at different wavelengths. By comparing the observed dipole amplitudes and directions among catalogs, they emphasized that the measured dipole cannot be trivially interpreted as purely kinematic, and must be understood as a combination of kinematic, local-structure, and possible systematic contributions.

Despite this progress, most theoretical discussions of the kinematic dipole in number counts still rely on the highly idealized assumptions leading to equation (2). In real surveys, however,

- the number counts generally deviate significantly from a pure power law,
- spectral energy distributions (SEDs) vary substantially from source to source and cannot be described by a single spectral index,
- observations are performed through finite instrumental bandpasses,
- detection limits and selection criteria are often direction dependent and may even be stochastic.

With the advent of large, deep, multi-band surveys, it is becoming essential to incorporate these non-ideal features explicitly at the level of the theoretical formulation in order to interpret kinematic dipole measurements in a robust manner (schematically described in Fig. 1).

An important point to emphasize is that, while much of the existing literature has carefully investigated the behavior of dipole *estimators* (e.g., the impact of masks, incompleteness, calibration errors, and weighting schemes), the theoretical side has continued to rely on the strong simplifications of power-law counts and a single spectral index. In contrast, the aim of this paper is to formulate the kinematic dipole starting from a general number-count distribution and a general SED, including finite bandpasses, and to express the effect of the observer’s motion as a response of a multi-dimensional selection function. Specifically, we define the dipole amplitude as a functional acting on the selection function and the parent population, rather than as a single numerical coefficient. This formulation is designed to be directly portable to arbitrary catalog selections, including color cuts, photo- z selections, weights, and direction-dependent survey depths.

Throughout this paper, we assume that, in the cosmic rest frame (denoted by a prime), the source distribution is statistically isotropic and contains no intrinsic dipole component. This assumption defines the theoretical reference model used to evaluate the kinematic response to the observer’s motion. All anisotropies derived in the following are therefore attributed to the observer’s velocity and to the response of the observational and selection processes. In real finite catalogs, however, the dipole estimated from data may also contain contributions from large-scale structure and survey-dependent systematics; the separation between these effects and the kinematic response will be discussed explicitly in Section 8. The most direct reference for the kinematic dipole is the CMB dipole, which provides a precise estimate of the observer’s velocity vector $\vec{\beta}_{\text{CMB}}$.

Given this velocity, the theoretical framework developed in this paper predicts the expected dipole vector in source counts as

$$\vec{d}_{\text{kin}} \equiv \mathcal{A} \vec{\beta}_{\text{CMB}}. \quad (3)$$

In practice, however, the dipole vector \vec{d}_{est} estimated from a finite catalog may also contain contributions from large-scale structure and from observational systematics. The relation between the theoretical coefficient \mathcal{A} and the estimated dipole, as well as the associated statistical uncertainties, will be clarified in the main text and appendices.

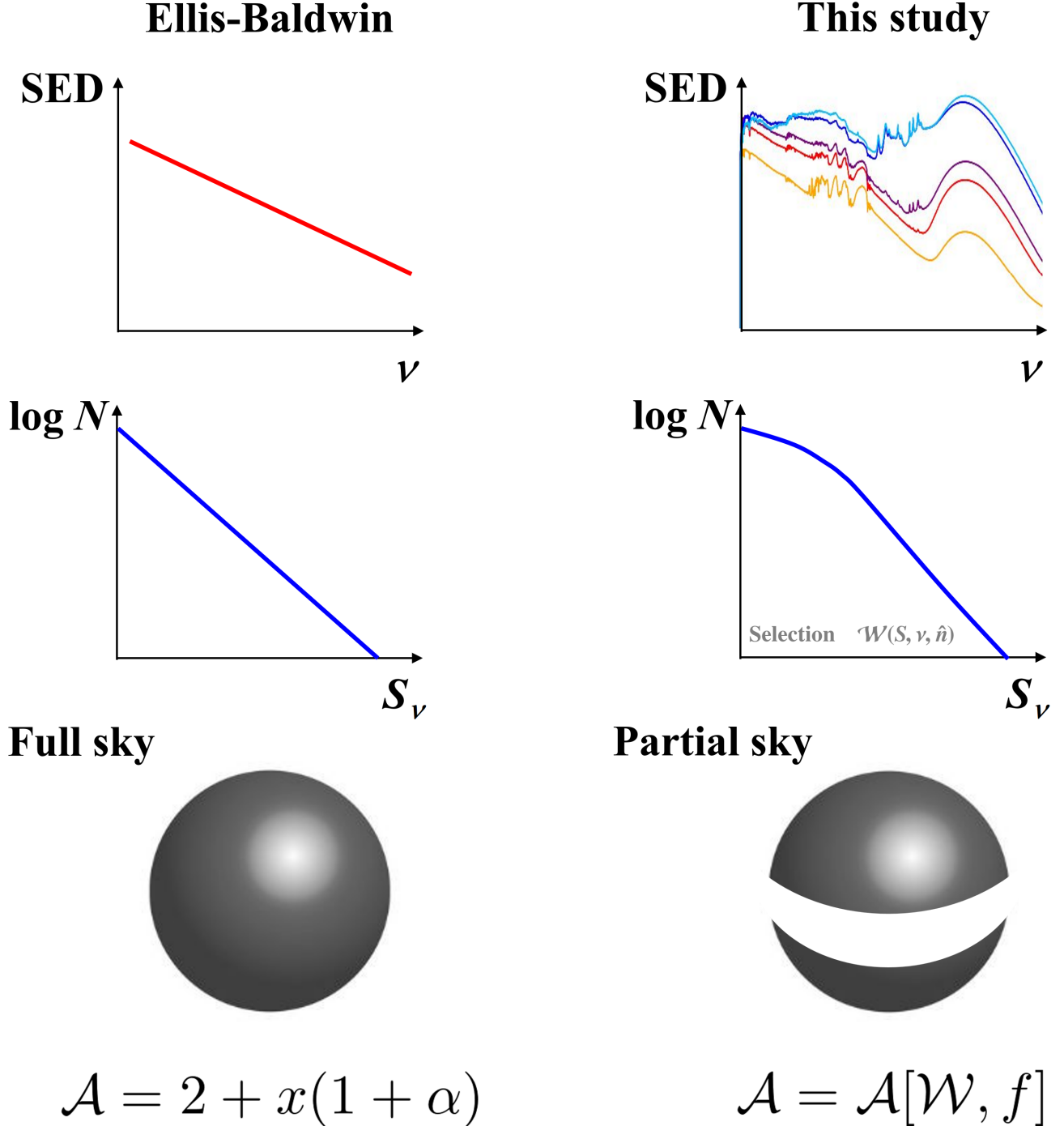


Figure 1. Schematic comparison between the classical Ellis–Baldwin formulation (left) and the general framework developed in this study (right). The classical approach assumes power-law number counts, a single power-law spectral energy distribution(SED), a sharp flux limit, and full-sky coverage, yielding a dipole amplitude $\mathcal{A} = 2 + x(1 + \alpha)$. In contrast, the present framework allows for general number counts, diverse SEDs, gradual or probabilistic selection, and incomplete sky coverage, all of which are absorbed into the functional dipole coefficient $\mathcal{A}[\mathcal{W}, f]$.

The structure of this paper is as follows. In Section 2, we introduce notation and define the relevant observables, including the treatment of band fluxes for general SEDs and filters (Section 2.3). In Section 3, we define a general, direction-dependent, multi-dimensional selection function $\mathcal{W}(\mathbf{y}, \hat{\mathbf{n}})$ and describe how the effect of observer motion can

be encoded as a mapping of observables, $\mathbf{y} \mapsto \mathbf{y}_\delta$. Section 4 derives the kinematic dipole to first order in the observer's velocity, showing that the dipole coefficient is given by a functional $\mathcal{A}[\mathcal{W}, f]$ representing the Doppler response of the selection function (equation (25)). In Section 5, we derive the flux-response coefficient q_b for general SEDs and filters, and present a practical implementation for finite catalogs (Section 5.3). Section 6 demonstrates how the response can be decomposed using the chain rule to accommodate color selections and photo- z selections. In Section 7, we show that the classical Ellis–Baldwin result is consistently recovered as a special limiting case through a sequence of controlled approximations. Section 8 discusses the connection between the theoretical coefficient \mathcal{A} and the dipole vector estimated from data (Section 8.1), and places existing observational tensions in context (Section 8.3). Additional details on statistical uncertainties and estimator properties are provided in the appendices (Appendices A and B).

2. DEFINITIONS OF NOTATION AND OBSERVABLES

2.1. Notation conventions

Throughout this paper, we adopt the following notation conventions.

- Three-dimensional vectors in real space (such as velocities, dipole vectors, and directions) are denoted by arrows, $\vec{\cdot}$.
- Elements of multi-dimensional parameter spaces are denoted by bold symbols, \mathbf{y} .
- A prime ('') indicates quantities defined in the cosmic rest frame.

2.2. Direction and Doppler factor

Let $\hat{\vec{n}}$ denote the direction of observation and $\vec{\beta}$ the velocity of the observer. We define the Doppler factor as

$$\delta(\hat{\vec{n}}) \equiv \frac{1}{\gamma(1 - \vec{\beta} \cdot \hat{\vec{n}})}, \quad \gamma \equiv (1 - \beta^2)^{-1/2}, \quad (4)$$

where $\beta \equiv |\vec{\beta}|$. For $\beta \ll 1$, the first-order expansion gives

$$\delta(\hat{\vec{n}}) = 1 + \vec{\beta} \cdot \hat{\vec{n}} + \mathcal{O}(\beta^2), \quad (5)$$

$$\ln \delta(\hat{\vec{n}}) = \vec{\beta} \cdot \hat{\vec{n}} + \mathcal{O}(\beta^2). \quad (6)$$

2.3. Band fluxes for general SEDs and filters

In this paper, the basic observables for each source are the fluxes measured in individual photometric bands, S_b . We first denote the spectral flux density in the cosmic rest frame by

$$S'_{\nu'}(\nu'; z, \psi), \quad (7)$$

where z is the redshift and ψ represents a set of intrinsic parameters characterizing the source SED.

When the same source is observed from the direction $\hat{\vec{n}}$ by a moving observer, the frequency transforms according to the Doppler factor as

$$\nu = \delta(\hat{\vec{n}}) \nu'. \quad (8)$$

In the galaxy and QSO catalogs considered in this work, individual sources are effectively unresolved (point-like) with respect to the angular resolution of the survey. In this case, the relevant observable is not the specific intensity I_ν , but the flux density integrated over the solid angle of the source,

$$S_\nu(\nu) \equiv \int I_\nu(\nu, \hat{\vec{n}}) d\Omega. \quad (9)$$

In special relativity, the ratio I_ν/ν^3 is Lorentz invariant, which implies

$$I_\nu(\nu, \hat{\vec{n}}) = \delta^3 I'_{\nu'} \left(\frac{\nu}{\delta}, \hat{\vec{n}}' \right). \quad (10)$$

At the same time, aberration transforms the solid-angle element as $d\Omega = \delta^{-2} d\Omega'$. As a result, the flux density of a point source transforms as

$$S_\nu(\nu) = \int I_\nu d\Omega = \delta \int I'_{\nu'} d\Omega' = \delta S'_{\nu'}(\nu/\delta). \quad (11)$$

Next, let $R_b(\nu)$ denote the transmission (response) function of photometric band b. The observed band flux in the observer frame is defined as

$$S_b \equiv \int_0^\infty R_b(\nu) S_\nu(\nu) d\nu. \quad (12)$$

Substituting equation (11) into equation (12), the deformation of S_b due to the observer's motion can be written as

$$\begin{aligned} S_b(\delta) &= \int_0^\infty R_b(\nu) \delta S'_{\nu'}(\nu/\delta; z, \psi) d\nu \\ &= \delta^2 \int_0^\infty R_b(\delta\nu') S'_{\nu'}(\nu'; z, \psi) d\nu'. \end{aligned} \quad (13)$$

In the second line, we have performed the change of variables $\nu' = \nu/\delta$. In the following, all derived quantities constructed from band fluxes (such as colors or photo-z estimates) will inherit their dependence on δ through this transformation of S_b .

3. GENERALIZATION OF SELECTION EFFECTS IN SOURCE CATALOGS

In practical astronomical surveys, whether a given source is included in the final catalog is not determined by a single flux threshold alone. Instead, a variety of conditions are typically combined, including photometric uncertainties, quality flags, star–galaxy separation, color selections based on multi-band photometry, photo-z estimation, as well as spatially varying survey depth and sky masks.

In this paper, we represent all such effects by a single selection function

$$\mathcal{W}(\mathbf{y}, \hat{n}) \in [0, 1]. \quad (14)$$

Here $\mathcal{W} = 1$ indicates that a source is always included in the catalog, while $\mathcal{W} = 0$ means that it is completely excluded. Intermediate values of \mathcal{W} represent probabilistic selection, such as incompleteness or weighting schemes.

We denote the set of physical and observational parameters characterizing a source by

$$\mathbf{y} = (z, \psi, S_{b_1}, S_{b_2}, \dots), \quad (15)$$

where z is the redshift, ψ denotes a set of intrinsic parameters describing the source SED, and S_b are the observed band fluxes. A key point is that each source may have its own individual SED, and no assumption of a universal spectral shape or a representative spectral index is made.

Definition of the parent population and reference frame—We define the parent population distribution in the cosmic rest frame as

$$f'(\mathbf{y}') d\mathbf{y}' \equiv \frac{dN}{d\Omega' d\mathbf{y}'} d\mathbf{y}'. \quad (16)$$

Throughout this paper, we assume that f' is statistically isotropic and contains no intrinsic dipole component.

In the following, we exploit the fact that the observer frame coincides with the rest frame at $\delta = 1$, and adopt the shorthand notation $\mathbf{y} \equiv \mathbf{y}'|_{\delta=1}$. The effect of the observer's motion is then treated entirely through the mapping of observables

$$\mathbf{y} \mapsto \mathbf{y}_\delta, \quad (17)$$

which is induced by the Doppler factor. With this choice, all effects of the motion are absorbed into the selection function, and no additional Jacobian factors need to be introduced in the parent distribution $f(\mathbf{y})$.

Examples of selection effects—All of the following survey-specific effects can be consistently encoded in $\mathcal{W}(\mathbf{y}, \hat{\vec{n}})$:

- direction-dependent deterministic detection limits, $S_b > S_{\min}(\hat{\vec{n}})$,
- color selections and star–galaxy separation based on multi-band photometry,
- redshift selections based on photo- z estimates,
- sky masks, such as Galactic plane avoidance,
- probabilistic selection due to completeness corrections or weighting schemes.

In this way, the formalism developed here is applicable to the most general setting, simultaneously accommodating source-dependent SEDs, non-power-law number counts, and direction-dependent deterministic or stochastic selection criteria.

4. GENERALIZED SELECTION FUNCTION AND THE KINEMATIC DIPOLE

4.1. General expression for number counts under observer motion

We begin by recalling that aberration transforms the solid-angle element as

$$d\Omega = \delta^{-2} d\Omega'. \quad (18)$$

As a result, the number counts per unit solid angle acquire a factor of δ^2 .

In addition, the observer’s motion induces a transformation of the observables, which we write schematically as

$$\mathbf{y} \mapsto \mathbf{y}_\delta. \quad (19)$$

For example, a band flux transforms as

$$S_b \mapsto S_b(\delta), \quad (20)$$

and any derived quantities constructed from fluxes (such as colors or photo- z estimates) are implicitly affected through this mapping.

Combining these effects, the observed surface density of sources in the observer frame can be written in the general form

$$n(\hat{\vec{n}}) = \delta^2(\hat{\vec{n}}) \int f(\mathbf{y}) \mathcal{W}(\mathbf{y}_\delta, \hat{\vec{n}}) d\mathbf{y}. \quad (21)$$

This expression serves as the starting point of the present analysis.

4.2. Functional form of the dipole coefficient

We now expand equation (21) to first order in the observer’s velocity, or equivalently to first order in $\ln \delta$. This yields

$$n(\hat{\vec{n}}) = n_0(\hat{\vec{n}}) + \left(\vec{\beta} \cdot \hat{\vec{n}} \right) \left[2n_0(\hat{\vec{n}}) + \int f(\mathbf{y}) \frac{d}{d \ln \delta} \mathcal{W}(\mathbf{y}_\delta, \hat{\vec{n}}) \Big|_{\delta=1} d\mathbf{y} \right] + \mathcal{O}(\beta^2), \quad (22)$$

where we have defined

$$n_0(\hat{\vec{n}}) \equiv \int f(\mathbf{y}) \mathcal{W}(\mathbf{y}, \hat{\vec{n}}) d\mathbf{y}. \quad (23)$$

The fractional fluctuation in the number counts can therefore be written as

$$\frac{n(\hat{\vec{n}}) - n_0(\hat{\vec{n}})}{n_0(\hat{\vec{n}})} = \mathcal{A}(\hat{\vec{n}}) \vec{\beta} \cdot \hat{\vec{n}}, \quad (24)$$

with the dipole coefficient given by

$$\mathcal{A}(\hat{\vec{n}}) \equiv 2 + \frac{1}{n_0(\hat{\vec{n}})} \int f(\mathbf{y}) \left. \frac{d}{d \ln \delta} \mathcal{W}(\mathbf{y}_\delta, \hat{\vec{n}}) \right|_{\delta=1} d\mathbf{y}. \quad (25)$$

The first term, equal to 2, is a universal contribution arising from aberration, while the second term represents the Doppler response of the selection function.

Equations (21)–(25) provide the most general formulation of the kinematic dipole in source number counts, explicitly accounting for the deformation of catalog selection induced by special-relativistic effects (aberration and Doppler boosting). In cosmological observations, additional effects such as magnification bias due to gravitational lensing or relativistic corrections to the number density associated with gravitational potentials may also contribute to anisotropies. These effects are conceptually independent of the kinematic dipole considered here and can be incorporated as separate correction terms if required. In the present work, we focus exclusively on the kinematic contribution arising from the observer's motion.

5. FLUX-RESPONSE COEFFICIENT FOR GENERAL SEDS AND FILTERS

5.1. Logarithmic derivative of the band flux

From equation (13), the band flux can be written as

$$S_b(\delta) = \delta^2 I_b(\delta), \quad (26)$$

$$I_b(\delta) \equiv \int_0^\infty R_b(\delta\nu') S'_{\nu'}(\nu'; z, \psi) d\nu'. \quad (27)$$

It immediately follows that

$$\frac{d \ln S_b}{d \ln \delta} = 2 + \frac{d \ln I_b}{d \ln \delta}. \quad (28)$$

Since we are interested only in the leading-order effect of the observer's motion ($\beta \ll 1$), this quantity is evaluated at $\delta = 1$, where the observer frame coincides with the cosmic rest frame. We therefore define

$$q_b(\psi) \equiv \left. \frac{d \ln S_b}{d \ln \delta} \right|_{\delta=1} = 2 + \left. \frac{d \ln I_b}{d \ln \delta} \right|_{\delta=1}, \quad (29)$$

and refer to q_b as the Doppler response coefficient of band b.

The coefficient $q_b(\psi)$ depends explicitly on the intrinsic SED parameters ψ of each object and quantifies how sensitively the observed band flux responds to the observer's motion. As shown below, this quantity enters directly into the amplitude of the kinematic dipole through the response of the selection function.

5.2. Explicit form of the filter-response term

The logarithmic derivative of $I_b(\delta)$ with respect to $\ln \delta$ can be evaluated explicitly. Differentiating under the integral sign yields

$$\begin{aligned} \frac{d I_b}{d \ln \delta} &= \delta \frac{d}{d \delta} \int_0^\infty R_b(\delta\nu') S'_{\nu'}(\nu'; z, \psi) d\nu' \\ &= \int_0^\infty [\delta\nu' R'_b(\delta\nu')] S'_{\nu'}(\nu'; z, \psi) d\nu', \end{aligned} \quad (30)$$

where R'_b denotes the derivative of the filter response with respect to its argument. Evaluating this expression at $\delta = 1$ gives

$$\left. \frac{d \ln I_b}{d \ln \delta} \right|_{\delta=1} = \frac{\int_0^\infty [\nu' R'_b(\nu')] S'_{\nu'}(\nu'; z, \psi) d\nu'}{\int_0^\infty R_b(\nu') S'_{\nu'}(\nu'; z, \psi) d\nu'}. \quad (31)$$

Together with equation (29), this expression allows the Doppler response coefficient q_b to be computed explicitly for an arbitrary SED and an arbitrary bandpass filter.

5.3. Implementation with a finite sample

In the previous sections, the kinematic dipole coefficient \mathcal{A} has been defined as an integral over the parent population distribution $f(\mathbf{y})$. While this representation is natural from a theoretical perspective, practical data analyses rely on catalogs containing a finite number of sources. In this subsection, we therefore show explicitly how the general expressions can be implemented using a discrete sample.

In observational data, the integral over $f(\mathbf{y})$ is approximated by a finite set of objects $\{\mathbf{y}_i\}_{i=1}^N$ representing the parent population in the cosmic rest frame. For each object located in direction $\hat{\vec{n}}_i$, we define the selection weight

$$w_i^{(0)} \equiv \mathcal{W}(\mathbf{y}_i, \hat{\vec{n}}_i). \quad (32)$$

The background surface density can then be approximated as

$$n_0 \approx \frac{1}{4\pi} \sum_{i=1}^N w_i^{(0)}. \quad (33)$$

Similarly, the Doppler-response term of the selection function can be discretized as

$$\int f(\mathbf{y}) \frac{d}{d \ln \delta} \mathcal{W}(\mathbf{y}_\delta, \hat{\vec{n}}) \Big|_{\delta=1} d\mathbf{y} \approx \sum_{i=1}^N \frac{d}{d \ln \delta} \mathcal{W}((\mathbf{y}_i)_\delta, \hat{\vec{n}}_i) \Big|_{\delta=1}. \quad (34)$$

As a result, the dipole coefficient can be evaluated directly from a finite catalog as

$$\mathcal{A} \approx 2 + \frac{\sum_i \frac{d}{d \ln \delta} \mathcal{W}((\mathbf{y}_i)_\delta, \hat{\vec{n}}_i) \Big|_{\delta=1}}{\sum_i \mathcal{W}(\mathbf{y}_i, \hat{\vec{n}}_i)}. \quad (35)$$

This expression provides the most direct numerical implementation of the theoretically defined functional $\mathcal{A}[\mathcal{W}, f]$, without invoking any power-law approximation for the number counts or assuming a single spectral index. It naturally incorporates object-by-object variations in SEDs, multi-band photometry, photo- z selection, and direction-dependent detection limits.

In the next section, we describe how the theoretical dipole coefficient \mathcal{A} computed in this manner is related to the dipole vector \vec{d}_{est} estimated directly from observational data.

6. EXPLICIT DECOMPOSITION OF THE SELECTION RESPONSE VIA THE CHAIN RULE

6.1. General form: $\mathcal{W} = \mathcal{W}(\vec{u}, \hat{\vec{n}})$

We consider the case in which the selection function depends on a set of observed quantities \vec{u} (e.g. fluxes, colors, photo- z , or morphological parameters), and can be written as

$$\mathcal{W}(\mathbf{y}, \hat{\vec{n}}) = \mathcal{W}(\vec{u}(\mathbf{y}), \hat{\vec{n}}). \quad (36)$$

Since the observer's motion induces a transformation $\vec{u} \mapsto \vec{u}_\delta$, the Doppler response of the selection function can be expanded using the chain rule as

$$\frac{d}{d \ln \delta} \mathcal{W}(\mathbf{y}_\delta, \hat{\vec{n}}) \Big|_{\delta=1} = \sum_k \frac{\partial \mathcal{W}}{\partial u_k} \frac{du_{k,\delta}}{d \ln \delta} \Big|_{\delta=1}. \quad (37)$$

Substituting this expression into the response term appearing in the dipole coefficient,

$$\int f(\mathbf{y}) \frac{d}{d \ln \delta} \mathcal{W}(\mathbf{y}_\delta, \hat{\vec{n}}) \Big|_{\delta=1} d\mathbf{y}, \quad (38)$$

we obtain

$$\int f(\mathbf{y}) \frac{d}{d \ln \delta} \mathcal{W}(\mathbf{y}_\delta, \hat{\vec{n}}) \Big|_{\delta=1} d\mathbf{y} = \sum_k \int f(\mathbf{y}) \frac{\partial \mathcal{W}}{\partial u_k} \frac{du_{k,\delta}}{d \ln \delta} \Big|_{\delta=1} d\mathbf{y}. \quad (39)$$

This expression highlights that the kinematic dipole amplitude is controlled by the product of two factors: the sharpness of the selection boundary (encoded in $\partial \mathcal{W} / \partial u_k$) and the Doppler response of the corresponding observable ($du_{k,\delta} / d \ln \delta$). In contrast to power-law approximations, this formulation allows object-level information to be incorporated directly into the theoretical prediction.

6.2. Representative example: flux-threshold selection

As the simplest and most common example, consider a deterministic flux cut of the form

$$\mathcal{W}(\mathbf{y}) = \Theta(S_b - S_{\min}) \mathcal{W}_{\text{other}}(\mathbf{y}), \quad (40)$$

where $\mathcal{W}_{\text{other}}$ denotes additional selection criteria. In this case,

$$\frac{\partial \mathcal{W}}{\partial S_b} = \delta_D(S_b - S_{\min}) \mathcal{W}_{\text{other}}(\mathbf{y}), \quad (41)$$

and equation (37) yields

$$\frac{d}{d \ln \delta} \mathcal{W}(\mathbf{y}_\delta) \Big|_{\delta=1} = \frac{dS_b(\delta)}{d \ln \delta} \Big|_{\delta=1} \delta_D(S_b - S_{\min}) \mathcal{W}_{\text{other}}(\mathbf{y}) + \dots, \quad (42)$$

where the ellipsis represents additional contributions arising from the Doppler response of other observables entering $\mathcal{W}_{\text{other}}$ (e.g. colors).

Using

$$\frac{dS_b(\delta)}{d \ln \delta} \Big|_{\delta=1} = q_b(\psi) S_b, \quad (43)$$

with q_b defined in equation (29), we see that the response integral is dominated by the differential number counts near the flux threshold.

6.3. Multi-band selection, color cuts, and photo-z selection

For more realistic catalogs, the vector \vec{u} typically consists of multiple band fluxes $\{S_b\}$ together with derived quantities such as colors and photometric redshifts. In this case, the Doppler response of the selection function becomes

$$\frac{d}{d \ln \delta} \mathcal{W}(\mathbf{y}_\delta) \Big|_{\delta=1} = \sum_b \frac{\partial \mathcal{W}}{\partial \ln S_b} q_b(\psi) + \frac{\partial \mathcal{W}}{\partial z_{\text{phot}}} \frac{dz_{\text{phot},\delta}}{d \ln \delta} \Big|_{\delta=1} + \dots \quad (44)$$

The first term represents the contribution mediated by the Doppler response coefficients q_b of the individual bands, while the second term captures the response of the photo-z estimator itself. Therefore, provided that the full selection pipeline (including estimators and classification algorithms) can be expressed as a function $\mathcal{W}(\mathbf{y}, \hat{\vec{n}})$, the kinematic dipole coefficient \mathcal{A} can be computed directly within the present framework.

7. RECOVERY OF THE ELLIS–BALDWIN FORMULATION VIA SUCCESSIVE IDEALIZATIONS

In this section, we start from the most general formulation of the kinematic dipole derived in the previous sections and introduce a sequence of idealized assumptions, in order to clarify how the classical Ellis–Baldwin result emerges as a special limiting case. The goal here is not to invalidate the traditional formulation, but rather to identify explicitly which assumptions remove which pieces of physical information.

7.1. Starting point: the most general dipole expression

From the results obtained above, the fractional fluctuation in the number counts induced by the observer’s motion can be written, to first order in the velocity, as

$$\frac{n(\hat{\vec{n}}) - n_0(\hat{\vec{n}})}{n_0(\hat{\vec{n}})} = \mathcal{A}(\hat{\vec{n}}) \vec{\beta} \cdot \hat{\vec{n}} + \mathcal{O}(\beta^2), \quad (45)$$

where the dipole coefficient is given by

$$\mathcal{A}(\hat{\vec{n}}) = 2 + \frac{1}{n_0(\hat{\vec{n}})} \int f(\mathbf{y}) \frac{d}{d \ln \delta} \mathcal{W}(\mathbf{y}_\delta, \hat{\vec{n}}) \Big|_{\delta=1} d\mathbf{y}. \quad (46)$$

The first term, equal to 2, is the universal contribution from aberration, while the second term encodes the Doppler response of the selection function. This expression applies to the most general situation, including object-dependent SEDs, non-power-law number counts, and direction-dependent deterministic detection limits.

In what follows, we introduce a series of simplifying assumptions and examine how the above expression reduces step by step.

7.2. Approximation I: full-sky coverage and uniform completeness

We first consider the idealized case in which the entire sky is observed uniformly, with no mask and no spatial variation in depth or completeness. That is,

$$\mathcal{W}(\mathbf{y}, \hat{\vec{n}}) = \mathcal{W}(\mathbf{y}), \quad n_0(\hat{\vec{n}}) = \bar{n}_0. \quad (47)$$

In this limit, the dipole coefficient becomes independent of direction, $\mathcal{A}(\hat{\vec{n}}) \rightarrow \mathcal{A}$, and the fractional fluctuation reduces to a pure dipole,

$$\frac{n(\hat{\vec{n}}) - \bar{n}_0}{\bar{n}_0} = \mathcal{A} \vec{\beta} \cdot \hat{\vec{n}}. \quad (48)$$

7.3. Approximation II: deterministic flux-threshold selection

Next, we assume that the selection function is determined solely by a single flux threshold measured in a given band,

$$\mathcal{W}(\mathbf{y}) = \Theta(S_b - S_{\min}). \quad (49)$$

In this case, application of the chain rule gives

$$\frac{d}{d \ln \delta} \mathcal{W}(\mathbf{y}_\delta) \Big|_{\delta=1} = \frac{dS_b(\delta)}{d \ln \delta} \Big|_{\delta=1} \delta_D(S_b - S_{\min}). \quad (50)$$

As a result, the response term in equation (46) is controlled by the differential number counts in the vicinity of the flux threshold.

It is therefore natural to define

$$x \equiv - \frac{d \ln N(> S)}{d \ln S} \Big|_{S_{\min}}, \quad (51)$$

where $N(> S)$ denotes the cumulative number counts. With this convention, a pure power-law form $N(> S) \propto S^{-x}$ corresponds to a constant positive value of x , avoiding any ambiguity in sign. The dipole coefficient then becomes

$$\mathcal{A} = 2 + x \frac{d \ln S_b}{d \ln \delta} \Big|_{\delta=1}. \quad (52)$$

7.4. Approximation III: from band flux to effective flux density

The original Ellis–Baldwin expression is formulated in terms of a flux density measured at a reference frequency. In contrast, the quantity S_b used here is a band-integrated observable defined through an arbitrary filter response $R_b(\nu)$. Depending on the normalization of R_b , S_b may represent either a band-averaged flux density or an integrated band flux.

To make contact with the Ellis–Baldwin form, we introduce the *effective flux density*

$$S_{b,\nu} \equiv \frac{S_b}{\Delta_b}, \quad \Delta_b \equiv \int_0^\infty R_b(\nu) d\nu. \quad (53)$$

Here Δ_b is a fixed effective bandwidth that does not depend on the Doppler factor δ . If the filter is normalized such that $\int R_b(\nu) d\nu = 1$, then $S_{b,\nu} = S_b$.

Since Δ_b is independent of δ , it follows immediately that

$$\frac{d \ln S_{b,\nu}}{d \ln \delta} \Big|_{\delta=1} = \frac{d \ln S_b}{d \ln \delta} \Big|_{\delta=1}. \quad (54)$$

Thus, the apparent difference between band fluxes and flux densities is purely notational, and does not affect the form of the dipole coefficient.

7.5. Approximation IV: narrow band and single spectral index

We now assume that the observational band is sufficiently narrow, and that the intrinsic spectrum of each source can be approximated near the band by a single power law,

$$S'_{\nu'}(\nu') \propto \nu'^{-\alpha}. \quad (55)$$

The Ellis–Baldwin derivation concerns unresolved point sources. For such sources, the invariance of I_ν/ν^3 together with aberration implies that the observed flux density transforms as

$$S_\nu(\nu) = \delta S'_{\nu'}(\nu/\delta), \quad (56)$$

which is equivalent to the transformation derived earlier in equation (11). Under the power-law approximation, this gives

$$S_\nu(\nu) \propto \delta (\nu/\delta)^{-\alpha} \propto \delta^{1+\alpha}. \quad (57)$$

In the narrow-band limit, the effective flux density $S_{b,\nu}$ coincides with S_ν evaluated at the band center, and therefore

$$\left. \frac{d \ln S_{b,\nu}}{d \ln \delta} \right|_{\delta=1} = 1 + \alpha. \quad (58)$$

7.6. Approximation V: power-law number counts

Finally, we assume that the cumulative number counts, expressed in terms of the effective flux density, follow a power law,

$$N(> S_{b,\nu}) \propto S_{b,\nu}^{-x}. \quad (59)$$

In this limit, the slope parameter x defined in equation (51) is a constant, and all detailed information about the selection boundary is compressed into a single number.

7.7. Recovery of the Ellis–Baldwin formulation

Imposing approximations I–V simultaneously (full-sky uniform coverage, deterministic flux threshold, effective flux density, narrow band with a single spectral index, and power-law number counts), equations (52) and (58) combine to give

$$\mathcal{A} = 2 + x(1 + \alpha). \quad (60)$$

The corresponding kinematic dipole vector is therefore

$$\vec{d}_{\text{kin}} = [2 + x(1 + \alpha)] \vec{\beta}, \quad (61)$$

which reproduces exactly the classical result of G. F. R. Ellis & J. E. Baldwin (1984).

7.8. What is lost and what is retained

This recovery procedure makes explicit which physical information is discarded when adopting the Ellis–Baldwin formulation:

- object-to-object variations in SEDs,
- curvature of the number counts,
- multi-band photometry, color cuts, and photo- z information,
- direction-dependent detection limits and weighting schemes.

The general formulation developed in this work retains all of these effects and provides a unified framework for evaluating the kinematic dipole without relying on power-law approximations. The Ellis–Baldwin result is naturally recovered as a well-defined limiting case.

8. DISCUSSION AND CONCLUSIONS

8.1. Estimating the dipole direction and amplitude from real data

Up to this point, we have shown that the kinematic effect of the observer’s motion leads to a dipolar modulation of the number counts,

$$\frac{n(\hat{\vec{n}}) - n_0(\hat{\vec{n}})}{n_0(\hat{\vec{n}})} = \mathcal{A}(\hat{\vec{n}}) \vec{\beta} \cdot \hat{\vec{n}} + \mathcal{O}(\beta^2), \quad (62)$$

where $\mathcal{A}(\hat{\vec{n}})$ is the dipole coefficient defined in equation (25). In this section, we describe concrete procedures for estimating the dipole direction and amplitude directly from observational catalogs.

Before entering the methodology, it is useful to recall that the observed dipole in source number counts may contain several distinct contributions. The dipole vector estimated from data, \vec{d}_{est} , generally includes not only the kinematic component \vec{d}_{kin} , but also an intrinsic component arising from large-scale structure within a finite survey volume, \vec{d}_{LSS} , as well as contributions from observational systematics such as photometric calibration errors, mask incompleteness, or stellar contamination, \vec{d}_{sys} . Conceptually, one may therefore write

$$\vec{d}_{\text{est}} = \vec{d}_{\text{kin}} + \vec{d}_{\text{LSS}} + \vec{d}_{\text{sys}}. \quad (63)$$

This decomposition reflects the interpretation advocated by [C. Gibelyou & D. Huterer \(2012\)](#), who emphasized that observed number-count dipoles in realistic catalogs generally include non-kinematic contributions in addition to the kinematic signal. The WISE AGN analysis by [A. K. Singal \(2021\)](#) provides a concrete example in which the commonly used kinematic coefficient cannot be unambiguously specified by a single number. The complex mid-infrared selection, combined with diverse AGN SEDs, directly motivates a formulation in which the kinematic response is treated as a functional of the selection function and the parent population. The theoretical framework developed in this paper provides the prediction $\vec{d}_{\text{kin}} = \mathcal{A}\vec{\beta}$, while the assessment and mitigation of \vec{d}_{LSS} and \vec{d}_{sys} are survey-specific tasks, typically addressed using mock catalogs, tomographic analyses, and null tests.

A crucial point is that what is directly inferred from observations is the dipole vector itself. Theory provides a prediction for the kinematic contribution in the form $\vec{d}_{\text{kin}} \equiv \mathcal{A}\vec{\beta}$ to first order in the velocity. This viewpoint, treating the dipole vector as the primary observable and separating its physical interpretation, is consistent with the survey-to-survey comparisons emphasized by [C. Gibelyou & D. Huterer \(2012\)](#). In our formulation, this separation is sharpened further by making the kinematic amplitude explicitly survey dependent through the functional $\mathcal{A}[\mathcal{W}, f]$.

In what follows, we therefore focus on explicit estimators for the dipole *direction* and *amplitude* from a finite source catalog. Closely related estimators have been used in previous analyses (e.g. [F. Crawford 2009](#); [M. Rubart & D. J. Schwarz 2013](#); [P. Tiwari et al. 2015](#)), and here we clarify how they connect to the generalized dipole coefficient \mathcal{A} derived in this work.

The coefficient \mathcal{A} introduced above plays a role that is conceptually distinct from that of the dipole estimator itself. Rather than being a single numerical constant, \mathcal{A} is a *functional* of the parent population distribution $f(\mathbf{y})$ and the selection function $\mathcal{W}(\mathbf{y}, \hat{\vec{n}})$,

$$\mathcal{A} \equiv \mathcal{A}[\mathcal{W}, f]. \quad (64)$$

This functional nature implies that the statistical uncertainty and detection significance of the estimated dipole vector \vec{d}_{est} are not determined solely by the total number of sources, but depend fundamentally on how the survey selection and the underlying population enter the theoretical prediction. A quantitative discussion of this point is provided in Appendix B, where the error covariance of the dipole estimator is derived using the Fisher information matrix based on a Poisson likelihood. There we show explicitly how the geometric sensitivity encoded by the survey mask and completeness is related to the structure of the estimator and to the functional form of $\mathcal{A}[\mathcal{W}, f]$.

8.1.1. Definition of the dipole vector

We define the fractional fluctuation in the number counts as

$$\Delta(\hat{\vec{n}}) \equiv \frac{n(\hat{\vec{n}}) - \bar{n}}{\bar{n}}, \quad (65)$$

where \bar{n} denotes the all-sky mean (or the mean under the survey mask). The $\ell = 1$ component can then be written as

$$\Delta(\hat{\bar{n}}) \simeq \vec{d} \cdot \hat{\bar{n}}, \quad (66)$$

where the dipole vector is parameterized as

$$\vec{d} = d \hat{\vec{d}}, \quad d \equiv |\vec{d}|, \quad \hat{\vec{d}} \equiv \vec{d}/|\vec{d}|. \quad (67)$$

Here $\hat{\vec{d}}$ denotes the dipole direction and d its amplitude. For a purely kinematic origin, one expects

$$\vec{d}_{\text{kin}} \simeq \mathcal{A} \vec{\beta}. \quad (68)$$

8.1.2. Least-squares estimation for a finite catalog

Consider a catalog of N sources with observed directions $\{\hat{\bar{n}}_i\}_{i=1}^N$, optionally assigned weights w_i . Let $W(\hat{\bar{n}})$ denote the effective survey window including masks and depth variations, and let $\lambda(\hat{\bar{n}})$ be the corresponding expected surface density. As a starting point, we fit the observed fluctuation field with the model

$$\Delta_{\text{obs}}(\hat{\bar{n}}) \simeq \vec{d} \cdot \hat{\bar{n}}. \quad (69)$$

In practice, the sky may be discretized into sufficiently fine pixels. Adopting a general linear least-squares approach, we minimize the loss function

$$\chi^2(\vec{d}) \equiv \sum_p \omega_p \left[\Delta_p - \vec{d} \cdot \hat{\bar{n}}_p \right]^2, \quad (70)$$

where p labels pixels, Δ_p is the estimated fractional fluctuation in pixel p , and ω_p is a weight (e.g. $\omega_p \propto N_p$ for Poisson variance).

Setting $\partial\chi^2/\partial d_i = 0$ leads to the normal equations

$$\sum_j M_{ij} d_j = h_i, \quad (71)$$

$$M_{ij} \equiv \sum_p \omega_p \hat{n}_{p,i} \hat{n}_{p,j}, \quad (72)$$

$$h_i \equiv \sum_p \omega_p \Delta_p \hat{n}_{p,i}. \quad (73)$$

The solution is

$$\vec{d}_{\text{est}} = \mathbf{M}^{-1} \vec{h}. \quad (74)$$

The estimated direction and amplitude are then

$$\hat{\vec{d}}_{\text{est}} = \frac{\vec{d}_{\text{est}}}{|\vec{d}_{\text{est}}|}, \quad d_{\text{est}} = |\vec{d}_{\text{est}}|. \quad (75)$$

This least-squares estimator is equivalent to maximum-likelihood estimation under the assumption of Poisson-distributed number counts; a detailed derivation is given in Appendix A. Closely related treatments can be found in F. Crawford (2009) and M. Rubart & D. J. Schwarz (2013).

8.1.3. Using \mathcal{A} to compare with velocities and the CMB dipole

If the theoretical coefficient \mathcal{A} is known, the observed dipole can be mapped to an effective velocity. Assuming a purely kinematic origin,

$$\vec{d}_{\text{est}} \simeq \mathcal{A} \vec{\beta}, \quad (76)$$

which implies

$$\vec{\beta}_{\text{est}} \simeq \frac{\vec{d}_{\text{est}}}{\mathcal{A}}, \quad \beta_{\text{est}} = \frac{d_{\text{est}}}{\mathcal{A}}, \quad \hat{\vec{\beta}}_{\text{est}} = \hat{\vec{d}}_{\text{est}}. \quad (77)$$

Alternatively, adopting the velocity vector inferred from the CMB dipole, $\vec{\beta}_{\text{CMB}}$, one may predict

$$d_{\text{pred}} = \mathcal{A} |\vec{\beta}_{\text{CMB}}|, \quad \hat{d}_{\text{pred}} = \hat{\vec{\beta}}_{\text{CMB}}, \quad (78)$$

and compare with observations through the amplitude ratio $|d_{\text{est}}|/d_{\text{pred}}$ and the angular separation $\cos^{-1}(\hat{d}_{\text{est}} \cdot \hat{\vec{\beta}}_{\text{CMB}})$.

8.1.4. Practical treatment of the background density

Construction of Δ_p in equation (70) requires an estimate of the background (expected) surface density. In practice, one often writes

$$\lambda(\hat{\vec{n}}) = \bar{n} W(\hat{\vec{n}}) C(\hat{\vec{n}}), \quad (79)$$

where W denotes the geometric mask and C the effective completeness (including depth variations and stellar contamination). The fluctuation is then defined as

$$\Delta_p \equiv \frac{N_p - \lambda_p}{\lambda_p}. \quad (80)$$

Within the general formulation developed here, all such effects can be absorbed into a single effective selection function $\mathcal{W}(\mathbf{y}, \hat{\vec{n}})$. Specifically, the commonly used factorization $W(\hat{\vec{n}})C(\hat{\vec{n}})$ corresponds to the $\hat{\vec{n}}$ -dependent part of \mathcal{W} after marginalization over the source properties \mathbf{y} . From the estimator's point of view, however, the procedure reduces to a simple prescription: construct the difference between observed counts and expectation, and fit it linearly to $\vec{d} \cdot \hat{\vec{n}}$.

8.1.5. Practical evaluation of the theoretical coefficient \mathcal{A}

We have shown how the dipole vector \vec{d}_{est} can be estimated directly from a finite catalog. If the dipole is assumed to be of kinematic origin, theoretical interpretation in terms of a physical velocity requires an independent evaluation of \mathcal{A} .

In the general formulation of this work, \mathcal{A} is not a constant, but a functional of the selection function and the parent population distribution,

$$\mathcal{A} = 2 + \frac{1}{n_0} \int f(\mathbf{y}) \left. \frac{d}{d \ln \delta} \mathcal{W}(\mathbf{y}_\delta, \hat{\vec{n}}) \right|_{\delta=1} d\mathbf{y}, \quad (81)$$

as given in equation (25). In practice, this integral may be evaluated using

- numerical integration based on a model or external estimate of $f(\mathbf{y})$,
- a discrete-sum approximation using the catalog itself or a representative training sample (see Section 5.3),
- semi-analytic approaches combining SED templates with gradients of the selection function.

A key point is that the evaluation of \mathcal{A} does not affect the dipole estimator itself; it enters only at the stage where the estimated dipole vector is mapped to a physical velocity. As a result, the inferred dipole *direction* is independent of \mathcal{A} , while the physical interpretation of the *amplitude* depends directly on its accuracy.

The main theoretical contribution of this work lies in providing a consistent definition of \mathcal{A} for arbitrary SEDs and arbitrary selection functions. The classical Ellis–Baldwin formulation is recovered as a special limiting case.

8.2. Tension in observed dipole measurements

Recent measurements of the kinematic dipole using galaxy and QSO catalogs span radio, infrared, and optical surveys. While the observed dipole is often broadly aligned with the CMB dipole, a number of studies have reported amplitudes and/or directions that show partial disagreement with the CMB-based expectation, leading to a certain

level of tension in the literature. As emphasized by [C. Gibelyou & D. Huterer \(2012\)](#) through survey-to-survey comparisons, such discrepancies need not indicate a breakdown of the kinematic interpretation: they can plausibly arise from non-kinematic contributions, including local-structure effects and survey-dependent systematics. The excess dipole amplitude reported for mid-infrared selected AGN samples ([A. K. Singal 2021](#)) further illustrates that apparent tensions with the CMB expectation need not imply a failure of the kinematic interpretation. Instead, they may reflect an incomplete theoretical treatment of the survey-dependent kinematic response, consistent with the framework developed in this work. This viewpoint motivates a clear separation between (i) estimator-side uncertainties and biases and (ii) the theory-side evaluation of the kinematic response coefficient.

In radio surveys, dipole amplitudes larger than the CMB expectation have been reported in some cases, while optical and infrared QSO catalogs sometimes exhibit different trends in both amplitude and direction. Even within a single catalog, the inferred dipole can vary depending on flux thresholds or weighting schemes. These discrepancies are often attributed to observational systematics or to intrinsic contributions from large-scale structure. For example, [J. D. Wagenveld et al. \(2025\)](#) analyzed galaxy number-count dipoles across multiple surveys and show that the observed signal can be decomposed into a kinematic component consistent with the CMB velocity and a significant residual non-kinematic dipole. Their results highlight that apparent dipole anomalies need not imply new physics, but can arise from survey-dependent contributions beyond pure kinematics. However, in many analyses, the theoretical amplitude is still evaluated using the simplified Ellis–Baldwin expression $2 + x(1 + \alpha)$.

8.2.1. *Role of the theoretical coefficient \mathcal{A}*

As demonstrated in this work, the kinematic dipole amplitude coefficient \mathcal{A} is not, in general, a single exponent, but a functional of the selection function and the parent population. Finite bandpasses, object-to-object SED variations, non–power-law number counts, and multi-dimensional selection criteria (such as color and photo- z cuts) all have a direct impact on \mathcal{A} .

Consequently, apparent discrepancies between dipole amplitudes measured in different surveys do not necessarily signal estimator bias or new physics. They may simply reflect the fact that *the same theoretical coefficient has been applied to catalogs with fundamentally different selection functions*.

8.2.2. *Division of responsibility between estimator and theory*

In dipole analyses, the quantity directly inferred from data is the dipole vector \vec{d}_{est} , while theory provides a prediction in the form $\vec{d}_{\text{kin}} = \mathcal{A}\vec{\beta}$. These two components play distinct roles.

The statistical variance and directional accuracy of \vec{d}_{est} are determined primarily by the number of sources, the sky coverage, and the geometry of the survey mask, and can be quantified using the Fisher matrix derived in [Appendix B](#). By contrast, the value of \mathcal{A} depends on the detailed construction of the catalog. Conflating these two aspects can lead to unnecessary confusion in the interpretation of observational results.

8.2.3. *Meaning of comparisons with the CMB dipole*

The CMB dipole provides a highly precise reference for the observer’s velocity. Dipole measurements from extragalactic source catalogs serve as an independent test of this velocity. However, unless the theoretical coefficient \mathcal{A} is evaluated consistently with the survey’s selection, a discrepancy in amplitude alone cannot be taken as compelling evidence for a physical inconsistency. The framework presented here allows one to compute *a survey-specific value of \mathcal{A}* , thereby redefining comparisons with the CMB dipole in a conceptually clearer manner.

8.3. *Summary and outlook*

In this paper, we have developed a unified theoretical framework for the kinematic dipole in source number counts, without relying on the traditional power-law approximations for number counts and spectral energy distributions. For a general parent population $f(\mathbf{y})$ and a general selection function $\mathcal{W}(\mathbf{y}, \hat{\vec{n}})$ —including finite bandpasses, multi-band photometry, color and photo- z selection, weighting schemes, and direction-dependent deterministic detection limits—we have shown that the dipole coefficient can be written as the functional

$$\mathcal{A}(\hat{\vec{n}}) = 2 + \frac{1}{n_0(\hat{\vec{n}})} \int f(\mathbf{y}) \left. \frac{d}{d \ln \delta} \mathcal{W}(\mathbf{y}_\delta, \hat{\vec{n}}) \right|_{\delta=1} d\mathbf{y}. \quad (82)$$

This expression explicitly identifies the dipole amplitude as the Doppler response of the selection function, providing a transparent interface between catalog construction and theory.

Through a sequence of idealizations, we have shown that the classical Ellis–Baldwin result is recovered as a well-defined limiting case. We have also clarified the relationship between the dipole vector estimated from data and the theoretical coefficient \mathcal{A} , making explicit the division of responsibility between estimator statistics and theoretical input.

Looking ahead, several directions are particularly important:

- making survey-specific selection functions \mathcal{W} explicit at the level of catalog construction pipelines (including color cuts, photo- z estimators, quality flags, and weighting), and evaluating $\mathcal{A}[\mathcal{W}, f]$ numerically using catalogs or training samples;
- quantifying and separating intrinsic large-scale-structure contributions \vec{d}_{LSS} and systematic effects \vec{d}_{sys} from the estimated dipole vector, using mocks, tomographic analyses, and null tests;
- standardizing the representation of direction-dependent depth and probabilistic completeness for future surveys such as LSST, Euclid, and SKA, in order to enable consistent comparisons of \mathcal{A} across catalogs.

By pursuing these steps systematically, comparisons with the CMB dipole can move from the use of a universal simplified coefficient to survey-specific predictions based on \mathcal{A} , thereby sharpening the interpretation of the currently reported tensions. Only after such effects are fully accounted for does it become meaningful to assess the possibility of new physics or intrinsic dipole components.

ACKNOWLEDGEMENTS

This work was supported by the JSPS Grant-in-Aid for Scientific Research (24H00247), and by the Joint Research Program (General Research 2) of the Institute of Statistical Mathematics, “Machine-Learning-Based Cosmogony: From Structure Formation to Galaxy Evolution”.

APPENDIX

A. EQUIVALENCE BETWEEN DIPOLE ESTIMATION BASED ON POISSON LIKELIHOOD AND LEAST-SQUARES FITTING

In this appendix, we show that the least-squares estimator used in Section 8.1 of the main text is naturally derived from the maximization of the likelihood based on Poisson statistics of object counts. Related discussions, from the viewpoints of dipole detectability and the properties of estimators, can be found in the literature (e.g. [F. Crawford 2009](#)).

A.1. *Description of object counts in the Poisson model*

We divide the celestial sphere into sufficiently fine pixels and denote by N_p the observed number of objects in pixel p . Under the dipole model, the corresponding expectation value (intensity function) is defined as

$$\lambda_p(\vec{d}) \equiv \bar{n} W(\hat{\vec{n}}_p) \left[1 + \vec{d} \cdot \hat{\vec{n}}_p \right], \quad (\text{A1})$$

where \bar{n} is the mean surface density, and $W(\hat{\vec{n}})$ represents the observational window function including the sky mask and effective completeness. Since we focus only on the kinematic dipole, the term $\vec{d} \cdot \hat{\vec{n}}_p$ is treated as a small first-order perturbation.

Assuming that the counts in each pixel follow independent Poisson distributions, the likelihood function is given by

$$\mathcal{L}(\vec{d}) = \prod_p \frac{\lambda_p(\vec{d})^{N_p}}{N_p!} \exp \left[-\lambda_p(\vec{d}) \right]. \quad (\text{A2})$$

The corresponding log-likelihood is

$$\ln \mathcal{L}(\vec{d}) = \sum_p \left[N_p \ln \lambda_p(\vec{d}) - \lambda_p(\vec{d}) - \ln N_p! \right]. \quad (\text{A3})$$

A.2. Likelihood maximization and the normal equations

Assuming that the dipole amplitude is small, we expand $\ln \lambda_p(\vec{d})$ to first order in \vec{d} :

$$\ln \lambda_p = \ln \left[\bar{n} W(\hat{\vec{n}}_p) \right] + \vec{d} \cdot \hat{\vec{n}}_p + \mathcal{O}(d^2). \quad (\text{A4})$$

Substituting this expansion into Eq. (A3) and setting the derivative with respect to d_i to zero, we obtain the score equation

$$\frac{\partial \ln \mathcal{L}}{\partial d_i} = \sum_p \left[N_p - \lambda_p(\vec{0}) \right] \hat{n}_{p,i} + \mathcal{O}(d) = 0, \quad (\text{A5})$$

where $\lambda_p(\vec{0}) = \bar{n} W(\hat{\vec{n}}_p)$.

Keeping terms consistently to first order, the condition for likelihood maximization reduces to the linear system

$$\sum_j M_{ij} d_j = h_i, \quad (\text{A6})$$

with

$$M_{ij} \equiv \sum_p \bar{n} W(\hat{\vec{n}}_p) \hat{n}_{p,i} \hat{n}_{p,j}, \quad (\text{A7})$$

$$h_i \equiv \sum_p \left[N_p - \bar{n} W(\hat{\vec{n}}_p) \right] \hat{n}_{p,i}. \quad (\text{A8})$$

Therefore, the dipole estimator obtained by likelihood maximization is

$$\vec{d}_{\text{est}} = \mathbf{M}^{-1} \vec{h}. \quad (\text{A9})$$

A.3. Equivalence with least-squares estimation

Using the second-order (Gaussian) approximation to the Poisson likelihood, the negative log-likelihood becomes

$$-2 \ln \mathcal{L} \simeq \sum_p \frac{(N_p - \lambda_p)^2}{\lambda_p} + \text{const.} \quad (\text{A10})$$

This expression is equivalent to a weighted least-squares fit with variance $\sigma_p^2 = \lambda_p$. Accordingly, the formulation used in the main text,

$$\chi^2 = \sum_p \omega_p \left[\Delta_p - \vec{d} \cdot \hat{\vec{n}}_p \right]^2, \quad \omega_p \propto \lambda_p, \quad (\text{A11})$$

can be understood as a natural approximation to likelihood maximization based on Poisson statistics.

B. DIPOLE AMPLITUDE AS A FUNCTIONAL AND STATISTICAL UNCERTAINTY

The main result of this paper is that the amplitude of the kinematic dipole is not given by a single index, but is instead expressed as a *functional*

$$\mathcal{A} \equiv \mathcal{A}[\mathcal{W}, f], \quad (\text{B12})$$

which depends on the selection function \mathcal{W} , the parent population distribution $f(\mathbf{y})$, and the family of spectral energy distributions (SEDs).

In this appendix, we summarize how the dipole vector \vec{d}_{est} estimated from observations acquires statistical uncertainty under a finite number of objects and partial sky coverage, given a specific functional \mathcal{A} . The key point is that while the structure of statistical errors is classical, their expectation value is determined by the functional \mathcal{A} .

B.1. Separation between theoretical input and observational model

As shown in the main text, under a first-order expansion in velocity, the observed fractional fluctuation field can be written as

$$\Delta(\hat{\vec{n}}) \equiv \frac{n(\hat{\vec{n}}) - n_0(\hat{\vec{n}})}{n_0(\hat{\vec{n}})} \simeq \mathcal{A}(\hat{\vec{n}}) \vec{\beta} \cdot \hat{\vec{n}}. \quad (\text{B13})$$

In the full-sky and uniform-completeness limit, $\mathcal{A}(\hat{\vec{n}}) \rightarrow \mathcal{A}$, and the theoretical prediction reduces to a single dipole vector,

$$\vec{d}_{\text{kin}} \equiv \mathcal{A} \vec{\beta}. \quad (\text{B14})$$

In the following, we evaluate the estimation error by treating \vec{d}_{kin} as a *known theoretical input*. That is, the statistical discussion in this appendix is independent of the construction of the functional \mathcal{A} , and the two are clearly separated.

B.2. Poisson likelihood and Fisher matrix: statistical structure given the functional \mathcal{A}

Dividing the sky into sufficiently fine pixels, the expected number of objects in pixel p is written as

$$\lambda_p(\vec{d}) \equiv \bar{n} W(\hat{\vec{n}}_p) \left[1 + \vec{d} \cdot \hat{\vec{n}}_p \right], \quad (\text{B15})$$

where $W(\hat{\vec{n}})$ is a purely geometrical and observational window function that includes the sky mask and effective completeness.

From the Poisson likelihood

$$\ln \mathcal{L}(\vec{d}) = \sum_p \left[N_p \ln \lambda_p(\vec{d}) - \lambda_p(\vec{d}) - \ln N_p! \right], \quad (\text{B16})$$

the Fisher matrix is obtained as

$$F_{ij} = \sum_p \bar{n} W(\hat{\vec{n}}_p) \hat{n}_{p,i} \hat{n}_{p,j}. \quad (\text{B17})$$

This matrix coincides with the normal matrix \mathbf{M} derived in the least-squares formulation in the main text.

By the Cramér–Rao inequality, the covariance of the dipole estimator is given by

$$\text{Cov}(d_i, d_j) = (F^{-1})_{ij}. \quad (\text{B18})$$

The important point to emphasize here is the clear division of roles:

- the Fisher matrix F_{ij} is determined solely by the geometry of the observed region and the sample size, while
- the functional \mathcal{A} determines the *mean value* of the estimated dipole.

That is,

$$\vec{d}_{\text{est}} = \mathcal{A} \vec{\beta} + (\text{statistical fluctuations}). \quad (\text{B19})$$

The novelty of this paper lies in providing the theoretical framework for the former term.

B.3. Classical limit and noise dipoles

In the full-sky and uniform-completeness limit, one finds

$$F_{ij} = \frac{\bar{N}}{3} \delta_{ij}, \quad \text{Cov}(d_i, d_j) = \frac{3}{\bar{N}} \delta_{ij}. \quad (\text{B20})$$

This statistical structure itself is classical and is shared with Ellis–Baldwin-type analyses.

What is essentially different in the present work is that different functionals \mathcal{A} are placed on the same Fisher matrix. In the power-law approximation, $\mathcal{A} = 2 + x(1 + \alpha)$ is given as a constant, whereas in the general theory, \mathcal{A} depends on the details of the selection function and the SEDs.

Even when no true dipole is present, a finite sample size leads to a noise dipole in the estimator \vec{d}_{est} . In the full-sky limit, the amplitude $d = |\vec{d}_{\text{est}}|$ follows a Maxwell distribution, allowing a statistical assessment of the observed amplitude. This appendix does not introduce a new Fisher matrix; rather, it is intended to clarify how the main result of this paper, that the dipole amplitude is a functional, connects to observational uncertainties.

REFERENCES

Ahn, K. 2025, Journal of Korean Physical Society, 86, 145,
doi: [10.1007/s40042-024-01255-9](https://doi.org/10.1007/s40042-024-01255-9)

Crawford, F. 2009, ApJ, 692, 887,
doi: [10.1088/0004-637X/692/1/887](https://doi.org/10.1088/0004-637X/692/1/887)

Ellis, G. F. R., & Baldwin, J. E. 1984, MNRAS, 206, 377,
doi: [10.1093/mnras/206.2.377](https://doi.org/10.1093/mnras/206.2.377)

Ferreira, P. d. S., & Quartin, M. 2021, PhRvL, 127, 101301,
doi: [10.1103/PhysRevLett.127.101301](https://doi.org/10.1103/PhysRevLett.127.101301)

Gibelyou, C., & Huterer, D. 2012, MNRAS, 427, 1994,
doi: [10.1111/j.1365-2966.2012.22032.x](https://doi.org/10.1111/j.1365-2966.2012.22032.x)

Rubart, M., & Schwarz, D. J. 2013, A&A, 555, A117,
doi: [10.1051/0004-6361/201321215](https://doi.org/10.1051/0004-6361/201321215)

Secrest, N. J., von Hausegger, S., Rameez, M., et al. 2021,
ApJL, 908, L51, doi: [10.3847/2041-8213/abdd40](https://doi.org/10.3847/2041-8213/abdd40)

Siewert, T. M., Schmidt-Rubart, M., & Schwarz, D. J. 2021, A&A, 653, A9, doi: [10.1051/0004-6361/202039840](https://doi.org/10.1051/0004-6361/202039840)

Singal, A. K. 2021, Universe, 7, 107,
doi: [10.3390/universe7040107](https://doi.org/10.3390/universe7040107)

Tiwari, P., Kothari, R., Naskar, A., Nadkarni-Ghosh, S., & Jain, P. 2015, Astroparticle Physics, 61, 1,
doi: [10.1016/j.astropartphys.2014.06.004](https://doi.org/10.1016/j.astropartphys.2014.06.004)

Wagenveld, J. D., von Hausegger, S., Klöckner, H.-R., & Schwarz, D. J. 2025, A&A, 697, A112,
doi: [10.1051/0004-6361/202453397](https://doi.org/10.1051/0004-6361/202453397)